SCIENTIFIC REPORTS

OPEN

SUBJECT AREAS:
SODIUM CHANNELS
SODIUM

Received
1 October 2014

Accepted
8 December 2014

Published
19 January 2015

Correspondence and requests for materials should be addressed to T.D. (t.dudev@chem.uni-sofia.bg) or C.L. (carmay@gate.sinica.edu.tw)

Ion Selectivity in the Selectivity Filters of Acid-Sensing Ion Channels

Todor Dudev[1,2] & Carmay Lim[1,3]

[1]Institute of Biomedical Sciences, Academia Sinica, Taipei 115, Taiwan, [2]Faculty of Chemistry and Pharmacy, Sofia University, Sofia 1164, Bulgaria, [3]Department of Chemistry, National Tsing Hua University, Hsinchu 300, Taiwan.

Sodium-selective acid sensing ion channels (ASICs), which belong to the epithelial sodium channel (ENaC) superfamily, are key players in many physiological processes (e.g. nociception, mechanosensation, cognition, and memory) and are potential therapeutic targets. Central to the ASIC's function is its ability to discriminate Na^+ among cations, which is largely determined by its selectivity filter, the narrowest part of an open pore. However, it is unclear how the ASIC discriminates Na^+ from rival cations such as K^+ and Ca^{2+} and why its Na^+/K^+ selectivity is an order of magnitude lower than that of the ENaC. Here, we show that a well-tuned balance between electrostatic and solvation effects controls ion selectivity in the ASIC1a SF. The large, water-filled ASIC1a pore is selective for Na^+ over K^+ because its backbone ligands form more hydrogen-bond contacts and stronger electrostatic interactions with hydrated Na^+ compared to hydrated K^+. It is selective for Na^+ over divalent Ca^{2+} due to its relatively high-dielectric environment, which favors solvated rather than filter-bound Ca^{2+}. However, higher Na^+-selectivity could be achieved in a narrow, rigid pore lined by three weak metal-ligating groups, as in the case of ENaC, which provides optimal fit and interactions for Na^+ but not for non-native ions.

Acid sensing ion channels (ASICs) are weakly voltage-dependent, Na^+-selective channels that belong to the degenerin or epithelial Na^+ channel (ENaC) superfamily of ion channels[1–3]. They are devised to sense extracellular protons and open when the external pH decreases, due very often to tissue acidosis resulting from inflammation, muscle ischemia or stroke[4–6]. Largely expressed in the central and peripheral nervous systems[7], ASICs play pivotal roles in several physiological processes such as nociception, mechanosensation, fear-related behavior, seizure termination, modulation of synaptic plasticity, cognition, and memory[6]. They are potential therapeutic targets for painkillers and drugs against ischemic stroke and panic disorder[6].

Central to the function of ASICs is their ability to selectively conduct the cognate Na^+ against a background of competing ions, in particular K^+ with the same net charge and Ca^{2+} with nearly identical ionic radius as Na^+ for the same coordination number. ASICs exhibit Na^+:K^+ selectivity ranging from 3 to 30:1[8–10] and generally do not conduct divalent ions. However, ASIC1a, unlike other subtypes, is also permeable to Ca^{2+} with a Na^+:Ca^{2+} permeability ratio of ~18[8]. Interestingly, although the ASIC channels are Na^+-selective, their Na^+:K^+ selectivity is an order of magnitude lower than that of the ENaC (the namesake originator of the ENaC/degenerin superfamily), which ranges from 100–500:1[3,11].

The metal ion selectivity of an ion channel is largely determined by its selectivity filter (SF), the narrowest part of an open pore lined with amino acid residues that face the pore lumen and interact specifically with the passing ion(s). The recent X-ray structure (PDB entry 4ntw, 2.07 Å) of an open-state ASIC1a in complex with snake toxin derived from Na^+-soaked crystals[12] has suggested a putative structure of an ASIC1a homotrimeric SF lined by Gly443 backbone peptide groups from the conserved Gly-Ala-Ser ("GAS") motif. However, it lacks electron density for Na^+ in the SF; nevertheless, the distance between the Gly443 backbone oxygen atoms of 6.2 Å, equivalent to a SF pore radius of ~3.6 Å, fits nicely fully hydrated Na^+ whose hydration radius has been estimated to be 3.58 Å[13]. The ASIC1a SF seems to be relatively flexible as it can adjust its geometrical parameters to accommodate the bulkier Cs^+: the mean distance between the Gly443 backbone oxygen atoms increases from 6.2 Å in the Na^+-soaked crystals to 7.1 Å in the Cs^+-bound SF (PDB entry 4nty, 2.65 Å)[12].

Because the SF pore radius is compatible with hydrated Na^+, the ASIC1a is thought to recognize fully hydrated metal ions and to discriminate among cations on the basis of the hydration ion size[12]. Thus, hydrated K^+ with a radius of ~4.2 Å would be too large to fit in the ASIC1a SF[12,14]. This raises the following intriguing questions: (1) Is the ion hydration sphere size the sole determinant of metal ion selectivity in ASICs? (2) Do other factors influence the competition between Na^+ and other monovalent (K^+) or divalent (Ca^{2+}) ions in these systems? If so, how do they control ion selectivity in the ASIC1a SF? Do the key determinants of Na^+ vs. K^+ selectivity in the ASIC1a SF

differ from those of Na^+ vs. Ca^{2+} selectivity? (3) Why is the ASIC1a SF less Na^+/K^+-selective compared to the ENaC SF?

Here, we endeavor to address these questions by evaluating the metal selectivity properties of model trimeric SFs of various pore sizes and compositions (see Methods). Since the interactions between the metal ions and ligands in the first and second coordination shell play a key role in the Na^+/K^+ and Na^+/Ca^{2+} competition, the structures of the metal-bound model SFs were subjected to all-electron geometry optimization without constraints using density functional theory. The fully optimized geometries were then used to compute the free energy for replacing K^+ or Ca^{2+} bound inside a model SF, $[K^+/Ca^{2+}(H_2O)_n$-filter], characterized by an effective dielectric constant x, with Na^+:

$$\left[Na(H_2O)_6\right]^+ + \left[K^+/Ca^{2+}(H_2O)_n - \text{filter}\right] + mH_2O \rightarrow$$

$$\left[Na^+(H_2O)_n - \text{filter}\right] + \left[K^+/Ca^{2+}(H_2O)_p\right] \qquad (1)$$

where n = 0, 6 or 7, m = 0 or 1, and p = 6 or 7. As the most common hydration number is six for Na^+ or K^+ and seven for Ca^{2+} in aqueous solution[15–18], hexahydrated Na^+ or K^+ and heptahydrated Ca^{2+} aqua complexes were modeled. The ion exchange free energy for eq 1 was computed as a sum of the gas-phase free energy ΔG^1 (electronic effects) and the solvation free energy difference between the products and reactants (solvation effects); i.e.,

$$\begin{aligned}\Delta G^x = \Delta G^1 &+ \Delta G_{solv}{}^x\left(\left[Na^+(H_2O)_n - \text{filter}\right]\right) \\ &+ \Delta G_{solv}{}^x\left(\left[K^+/Ca^{2+}(H_2O)_p\right]\right) \\ &- \Delta G_{solv}{}^x\left(\left[K^+/Ca^{2+}(H_2O)_n - \text{filter}\right]\right) \\ &- \Delta G_{solv}{}^x\left(\left[Na(H_2O)_6\right]\right) - m\Delta G_{solv}{}^x(H_2O)\end{aligned} \qquad (2)$$

A positive ΔG^x implies a K^+/Ca^{2+}-selective filter, whereas a negative value implies a Na^+-selective one. This approach (eq 2) has yielded trends in the free energy changes with varying parameters (e.g., the metal type, the metal hydration number, the ligand type, and the pore size) that are consistent with experimental findings[19–27]. Note that the contributions from other segments of the pore, kinetic barriers, or other ions in the surrounding baths to ion selectivity fall outside the scope of this work, as the aims herein are to identify the key determinants of Na^+/K^+ and Na^+/Ca^{2+} selectivity in the ASIC1a and ENaC SFs.

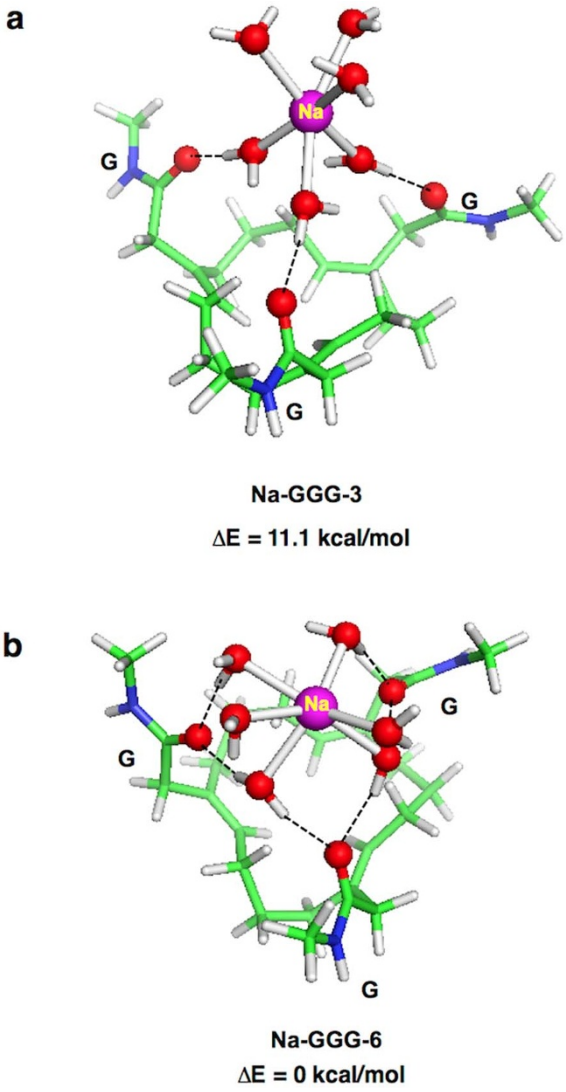

Figure 1 | B3LYP/6-31+G(3d,p) optimized structures and relative energies of formation (in kcal/mol) of $[Na(H_2O)_6]^+$-GGG SF complexes, characterized with (a) three and (b) six $H_2O\ldots O{=}C$ hydrogen bonds.

Results

Binding mode of metal hydrates to a model ASIC1a SF. *Na^+ complexes.* The model trimeric ASIC1a SF lined by three backbone peptide groups can bind hexahydrated Na^+ in two distinct modes (Figure 1): In the first binding mode, each of the three backbone oxygen atoms from the SF forms a hydrogen bond with a Na^+-bound water molecule, yielding three backbone–water hydrogen bonds (denoted as **Na-GGG-3**, Figure 1a). This binding mode requires a wide SF pore: the mean distance between backbone oxygen atoms for the **Na-GGG-3** complex is 6.8 Å. In the second binding mode, each SF backbone oxygen forms bifurcated hydrogen bonds with two Na^+-bound water molecules, yielding altogether six backbone–water hydrogen bonds (denoted as **Na-GGG-6**, Figure 1b). Relative to the **Na-GGG-3** complex, the increased number of hydrogen bonds in the **Na-GGG-6** complex increases the strength of electrostatic interactions and results in a more compact structure: the mean O–O distance between the SF backbone ligands decreases from 6.8 Å in the **Na-GGG-3** complex to 5.1 Å. Notably, the average backbone O–O distance in the **Na-GGG-3** and **Na-GGG-6** configurations (~6.0 Å) is close to the respective distance (6.2 Å) in the 4ntw crystal structure[12]. As the conformation with six hydrogen bonds (**Na-GGG-6**, Figure 1b) is energetically more favorable (by ~11 kcal/mol) than that with three hydrogen bonds (**Na-GGG-3**, Figure 1a), it was used for further evaluations (see below).

K^+ complexes. As for the Na^+ complexes, two distinct binding modes of hexahydrated K^+ to the model ASIC1a SF were also found with the binding mode containing three hydrogen bonds (**K-GGG-3**, Figure 2a) less stable than that with four hydrogen bonds (**K-GGG-4**, Figure 2b). Because K^+ is larger than Na^+ with longer K^+–O(water) bonds[28], only one of the backbone oxygen atoms can form bifurcated hydrogen bonds with two K^+-bound water molecules in the **K-GGG-4** complex (Figure 2b), hence the **K-GGG-4** complex contains four instead of six hydrogen bonds seen in the **Na-GGG-6** complex (Figure 1b). Consequently, the electronic energy of **K-GGG-4** is only ~4 kcal/mol lower than that of **K-GGG-3**, as compared to an energy difference of ~11 kcal/mol for the respective Na^+ complexes in Figure 1. Furthermore, the contraction of the SF upon $[K(H_2O)_6]^+$ binding in the **K-GGG-4** rather than the **K-GGG-3** complex is less than that upon $[Na(H_2O)_6]^+$ binding: the mean backbone O–O distance difference between **K-GGG-3** and **K-GGG-4** is 0.5 Å, whereas that between **Na-GGG-3** and **Na-GGG-6**

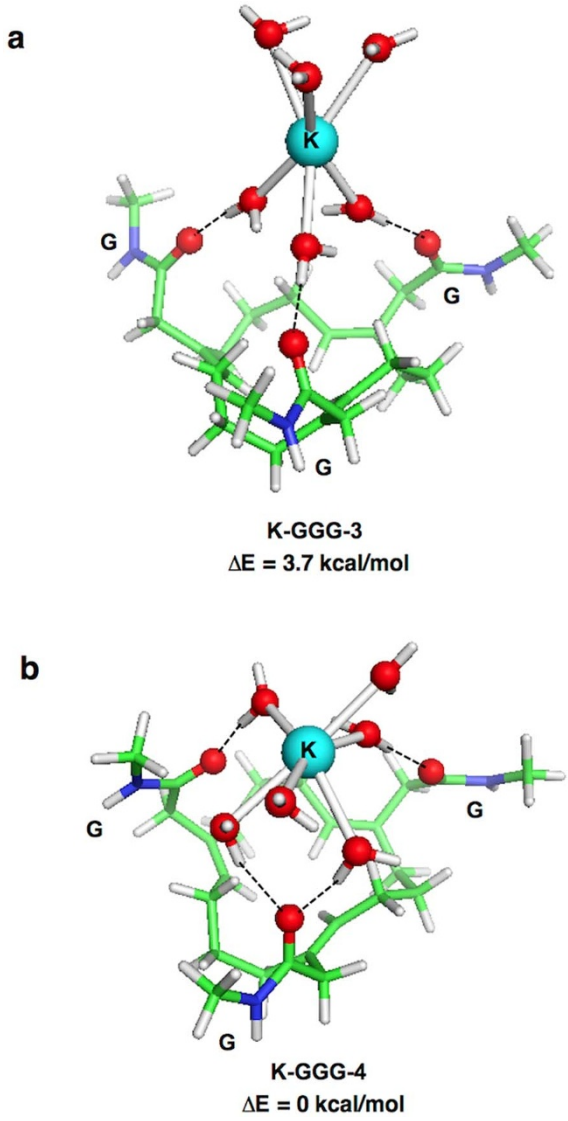

Figure 2 | B3LYP/6-31+G(3d,p) optimized structures and relative energies of formation (in kcal/mol) of $[K(H_2O)_6]^+$-GGG SF complexes, characterized with (a) three and (b) four $H_2O\ldots O{=}C$ hydrogen bonds.

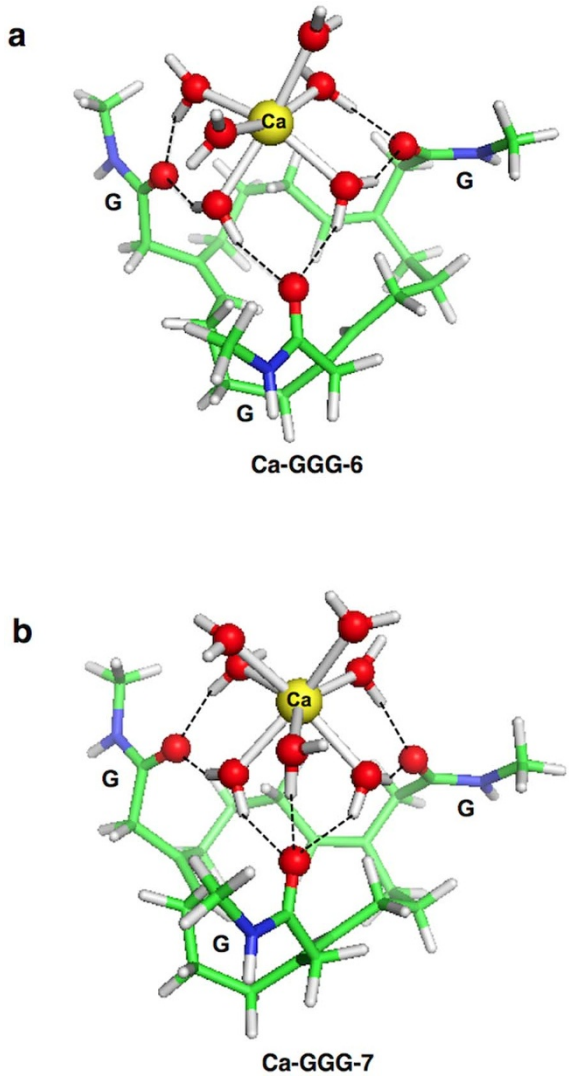

Figure 3 | B3LYP/6-31+G(3d,p) optimized structures of (a) $[Ca(H_2O)_6]^{2+}$-GGG SF and (b) $[Ca(H_2O)_7]^{2+}$-GGG SF complexes.

is 1.7 Å. This suggests that the number of HOH---O=C contacts is an important determinant of the structure and energetics of these systems.

Ca^{2+} complexes. As the ionic radius of hexa or heptacoordinated Ca^{2+} (1.00 or 1.06 Å) is similar to that of Na^+ (1.02 Å)[29], each of the three SF backbone oxygen atoms should be able to form bifurcated hydrogen bonds with water molecules. Indeed, each of the SF carbonyl oxygen atoms formed two hydrogen bonds with water ligands in the fully optimized structure of hexahydrated Ca^{2+} in the **GGG** SF (**Ca-GGG-6**, Figure 3a), but one of the carbonyl oxygen atoms formed hydrogen bonds with three water molecules in the optimized structure of *hepta*hydrated Ca^{2+} in the **GGG** SF (**Ca-GGG-7**, Figure 3b), which thus has an additional HOH---O=C hydrogen bond. Because of the stronger Ca^{2+}–OH_2---O=C electrostatic interactions, the Ca^{2+}-bound structures are quite compact with a mean SF O–O distance of 5.4 Å for **Ca-GGG-6** and 5.5 Å for **Ca-GGG-7**.

Competition among metal ions in the model ASIC1a SF. *Na^+ vs. K^+*. Substituting hydrated K^+ for hydrated Na^+ in the model ASIC1a SF is thermodynamically favorable: The ion exchange free energies are negative for an effective dielectric constant x ranging from 1 to 30 (–4.7 to –1.9 kcal/mol, Figure 4a), implying a Na^+-selective SF. Rigidifying the model ASIC1a SF, whose pore is optimized to fit hydrated Na^+, further disfavors the bulkier hydrated K^+ from binding, thus enhancing the competitiveness of Na^+: The metal exchange free energies in a Na^+-optimized **GGG** filter that is prohibited from relaxing upon binding K^+ (numbers in parentheses, Figure 4a) are even more negative (by 2.4 kcal/mol) than those in a **GGG** filter that can adjust to accommodate K^+. Since solvation effects ($x > 1$) diminished Na^+/K^+ selectivity (less negative ΔG^x with increasing x, Figure 4a), electronic factors favor binding of Na^+ over K^+ and govern the Na^+ vs. K^+ competition in the ASIC1a SF: Compared to K^+, Na^+ is a stronger Lewis acid and forms more polar and shorter bonds with water molecules. The much shorter Na^+–OH_2 (2.45 Å) bonds compared to K^+–OH_2 (2.82 Å) bonds allow the trimeric SF to gain more hydrogen-bond contacts with Na^+ than with K^+. This along with the more polarized Na^+–bound water molecules result in stronger electrostatic interactions with the SF carbonyl moieties.

Na^+ vs. Ca^{2+}. As the Ca^{2+} hydration number varies from 6 to 10 depending on the water:salt ratio, two Ca^{2+} hydration numbers were considered in the Ca^{2+} vs. Na^+ competition in the **GGG** SF: (1) hexahydrated Ca^{2+}, whose hydration number matches that of Na^+ (**Ca-GGG-6**, Figure 4b) and (2) heptahydrated Ca^{2+} (**Ca-GGG-7**,

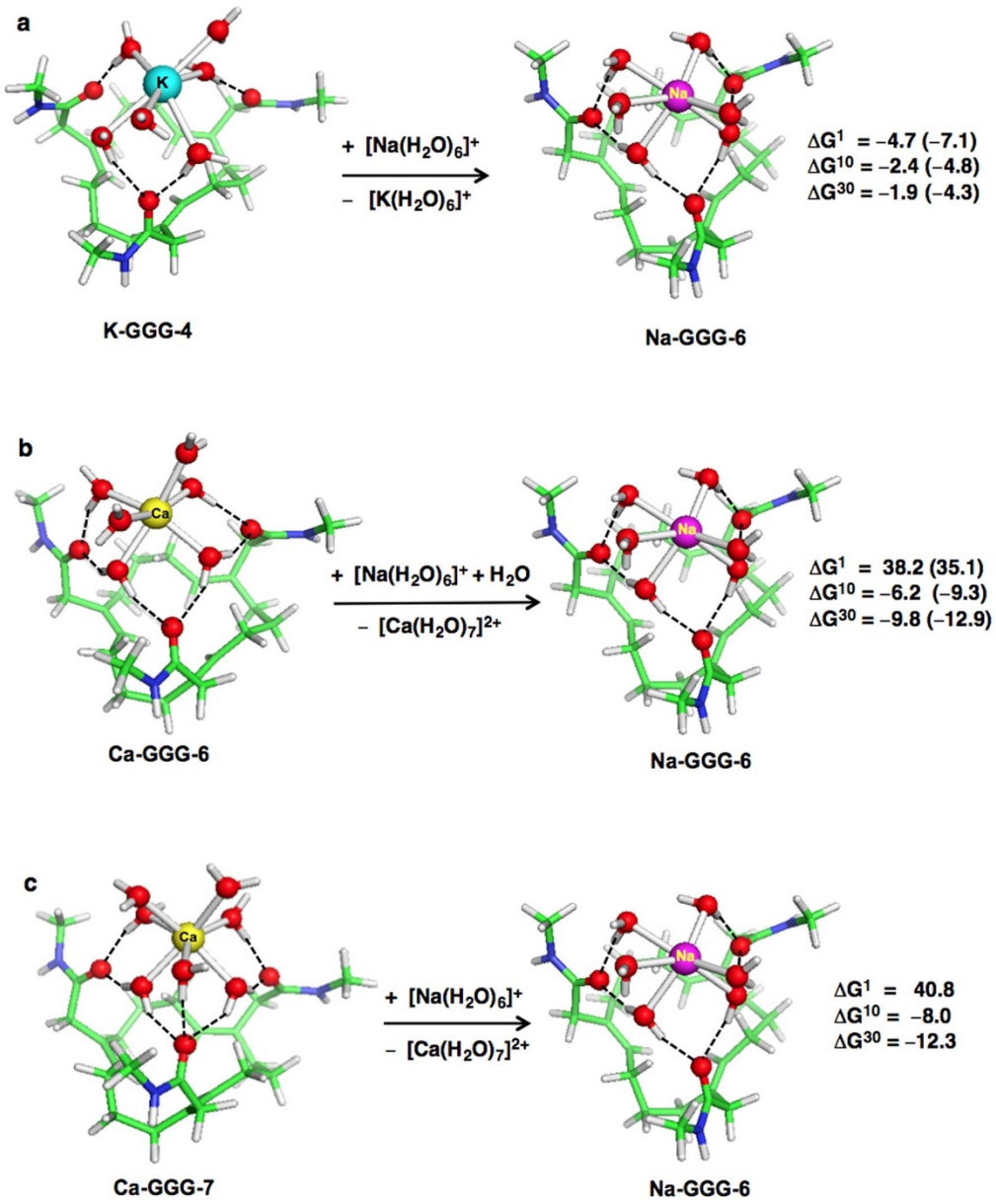

Figure 4 | The free energies, ΔG^x (in kcal/mol), for replacing (a) K^+ bound to 6 water molecules, (b) Ca^{2+} bound to six water molecules, and (c) Ca^{2+} bound to seven water molecules with Na^+ in the **GGG** ASIC model SF (eq 1). ΔG^1 refers to the metal exchange free energy in the gas phase, whereas ΔG^{10} and ΔG^{30} refer to the metal exchange free energies in an environment characterized by an effective dielectric constant of 10 and 30, respectively. The free energies for metal exchange in a rigid Na^+-optimized **GGG** filter prohibited from relaxing upon K^+/Ca^{2+} binding are in parentheses.

Figure 4c). Electronic effects again favor the better electron acceptor cation; i.e., divalent Ca^{2+} over monovalent Na^+ (positive ΔG^1 in Figures 4b,c). This is because divalent hydrated Ca^{2+} has stronger electrostatic interactions with the SF carbonyl moieties than hydrated Na^+. Thus, unlike the Na^+ vs. K^+ competition in the **GGG** SF, electronic effects *disfavor* the native Na^+ in the competition with Ca^{2+}.

Instead, a relatively high-dielectric environment in the ASIC1a SF is the key determinant of the Na^+/Ca^{2+} selectivity: Whereas the ion exchange free energy is positive in the gas phase (x=1), it is negative for an effective dielectric constant x ranging from 10 to 30 (–6.2 to –12.3 kcal/mol, Figures 4b,c). A high-dielectric environment in the ASIC1a SF favors binding of Na^+ over Ca^{2+} due mainly to the low desolvation penalty of the incoming Na^+ and the high free energy gain on solvating the outgoing Ca^{2+}: For x = 30 in eq 2, the solvation free energy difference between Ca^{2+} and Na^+ hydrates, $\Delta G_{solv}{}^x[Ca^{2+}(H_2O)_7] - \Delta G_{solv}{}^x[Na^+(H_2O)_6]$ = −136 kcal/mol, outweighs the difference between hydrated Na^+ and Ca^{2+} bound to the SF, $\Delta G_{solv}{}^x[Na^+(H_2O)_6$-filter$] - \Delta G_{solv}{}^x[Ca^{2+}(H_2O)_7$-filter$]$ = 83 kcal/mol, and the gas-phase free energy, ΔG^1 = 41 kcal/mol. Increasing the SF rigidity and metal hydration number both enhance Na^+/Ca^{2+} selectivity, albeit to a lesser extent than medium effects: The metal exchange free energies in a rigid **Na-GGG-6** pore (numbers in parentheses, Figure 4b) are more negative (by ~3 kcal/mol) than those in a flexible SF that can adjust to the geometrical requirements of hydrated Ca^{2+}. Furthermore, the free energies for replacing *hepta*hydrated Ca^{2+} with Na^+ in the **GGG** SF (Figure 4c) are more negative (by ~2 kcal/mol) than those for replacing *hexa*hydrated Ca^{2+} (Figure 4b).

Competition among metal ions in a model ENaC SF. Although ENaC and ASIC belong to the same superfamily of ion channels, the size and structure of their trimeric SFs appear to be quite different: Unlike the wide ASIC1a SF, the highly Na^+-selective asymmetric

ENaC SF is lined by conserved Ser residues and has a rigid, narrow pore (radius <2.5 Å) that fits dehydrated metal ions[30–32]. How does the ENaC SF select its cognate ion and achieve a Na^+/K^+ selectivity ratio (100–500) that is an order of magnitude greater than that exhibited by the ASIC SF (3–30)? No crystal structures are available for ENaC. Kellenberger et al.[33] proposed that the Ser backbone oxygen atoms interact with the permeating ion, whereas Sheng et al.[32] differ in proposing the α subunit's Ser hydroxyl oxygen to coordinate Na^+. Since it is unclear whether backbone or sidechain oxygen atoms or a combination of both coordinate the permeating ions, we modeled dehydrated ions bound in the two "limits" of the ENaC SFs: a **BBB** SF containing three backbone groups (Figure 5a) and a **SSS** SF lined by three Ser hydroxyl groups (Figure 5b). We then computed the free energies ΔG^x for Na^+ to displace K^+ (numbers in black) and Ca^{2+} (numbers in blue) in these two types of model SFs.

Na^+ vs. K^+. Higher Na^+/K^+ selectivity is achieved if backbone rather than Ser side chain oxygen atoms coordinate the metal cation: The free energies for replacing K^+ in the **BBB** SF with Na^+ (Figure 5a) are more favorable than those in the **SSS** SF (Figure 5b) by ~2 kcal/mol. Compared to the hydroxyl group, the carbonyl group has stronger charge-donating ability and interacts more favorably with Na^+ than K^+, thus helping to offset the larger Na^+ dehydration penalty. For both types of filters, Na^+/K^+ selectivity is dramatically enhanced if the ENaC SF were rigid. A rigid ENaC SF pore optimized to fit bare Na^+ strongly disfavors binding of the bulkier K^+, as evidenced by the much more negative $Na^+ \rightarrow K^+$ free energies (numbers in parentheses, Figure 5): A rigid, Na^+-optimized **BBB** SF enhances Na^+/K^+-selectivity by ~24 kcal/mol, whereas a rigid, Na^+-optimized **SSS** SF has a smaller effect (~19 kcal/mol).

In line with experimental findings, a rigid ENaC SF is more Na^+/K^+-selective than a rigid ASIC1a SF (the numbers in parentheses in Figure 5a are more negative than those in Figure 4a). Making the Na^+-binding site rigid in the ENaC structure enhanced Na^+/K^+-selectivity by an order of magnitude greater than rigidifying the Na^+-binding site in the ASIC1a structure: Na^+/K^+-selectivity is enhanced by ~24 kcal/mol in a rigid, constricted ENaC pore (Figure 5a), but by 2.4 kcal/mol in the rigid, wide ASIC1a pore (Figure 4a). This difference is mainly due to the smaller binding cavity in the ENaC SF compared to the ASIC1a one, as the same three backbone groups line the SFs of both types of channels.

Na^+ vs. Ca^{2+}. Unlike the competition between Na^+ and K^+, higher Na^+/Ca^{2+} selectivity was found in a **SSS** SF rather than a **BBB** SF: The $Na^+ \rightarrow Ca^{2+}$ free energies in the **SSS** SF (Figure 5b) are more favorable than those in the **BBB** SF (Figure 5a). This is mainly because the three weakly ligating Ser hydroxyl groups lining the narrow **SSS** SF "undercoordinate" Ca^{2+}, resulting in feeble interactions that cannot compensate for the cost of stripping the Ca^{2+}-bound water molecules, as evidenced by a $\Delta G^1 = -13$ kcal/mol, Figure 5b. As for the ASIC1a SF, the higher dielectric environment of the SF favors the permeating ion with the smaller dehydration penalty, thus Na^+ is preferred over Ca^{2+} in both **BBB** and **SSS** SFs (negative ΔG^x, $x \geq 10$, in Figure 5). Thus, a relatively high-dielectric SF providing suboptimal interactions for the rival dication can bestow high Na^+/Ca^{2+} selectivity.

Even though solvation effects favor Na^+ over Ca^{2+} in both the ENaC and ASIC1a SFs, the ENaC SF is more Na^+/Ca^{2+}-selective than the ASIC1a one. This is because in the wide ASIC1a SF, (i) there is no dehydration penalty and (ii) Ca^{2+} is no longer "undercoordi-

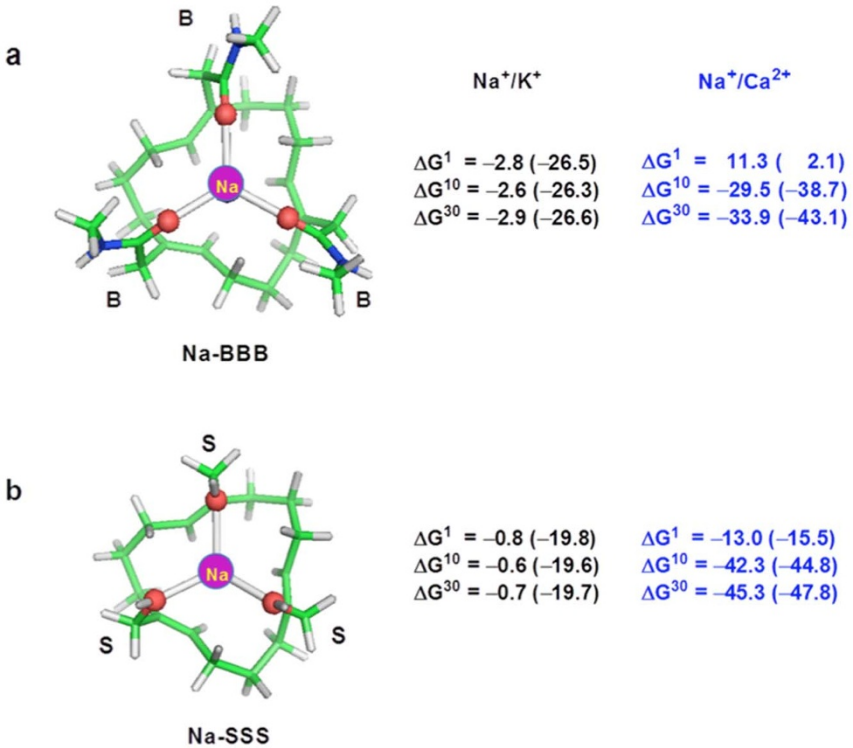

Figure 5 | The free energies, ΔG^x (in kcal/mol), for Na^+ to displace K^+ (numbers in black) and Ca^{2+} (numbers in blue) bound to (a) 3 $-CONHCH_3$ ligating groups (representing backbone peptide groups denoted by B) in the **BBB** filter and (b) 3 OH-ligating groups (representing Ser side chains) in the **SSS** filter (eq 1). ΔG^1 refers to the metal exchange free energy in the gas phase, whereas ΔG^{10} and ΔG^{30} refer to the metal exchange free energies in an environment characterized by an effective dielectric constant of 10 and 30, respectively. The free energies for metal exchange in a rigid Na^+-optimized **SSS** and **BBB** filters prohibited from relaxing upon K^+ or Ca^{2+} binding are in parentheses. Shown are B3-LYP/6-31+G(3d,p) fully optimized structures of Na^+ bound to the model SFs.

nated" but is bound to six (**Ca-GGG-6**, Figure 4b) or seven (**Ca-GGG-7**, Figure 4c) water molecules[34,35]. Thus, the gas-phase ΔG^1 free energy for replacing Ca^{2+} with Na^+ in the constricted ENaC SF (11 kcal/mol, Figure 5a) is less positive than that in the wide ASIC1a SF (38–41 kcal/mol, Figures 4b,c); consequently, in the higher dielectric SF ($x \geq 10$), the ΔG^x in Figure 5a (–30 to –34 kcal/mol) are more favorable than those in Figures 4b,c (–6 to –12 kcal/mol).

Discussion

Since the open-state structures with the native Na^+ ion bound in the SFs of the ASIC1a and ENaC have not yet been solved, we have examined the outcome of the competition among Na^+, K^+, and Ca^{2+} in models of these channel SFs, which were designed in accord with available experimental data (see Methods). Nevertheless, the results obtained are in line with experimental findings: The computed SF pore size, estimated by the area of the triangle formed by the metal-ligating oxygen atoms lining the SF, is consistent with the respective experimental estimate: (i) The calculated pore area of the model ENaC SF (6.3 Å^2 for **Na-BBB** or 6.9 Å^2 for **Na-SSS**, Figure 5) is consistent with the experimental estimate of $<$8.1 Å^2 [31]. (ii) The mean pore area of the **Na-GGG-3** and **Na-GGG-6** SFs in Figure 1 (15.7 Å^2) is also close to the respective area (16.6 Å^2) determined from the Na^+-bound ASIC1a/snake toxin crystal structure[12]. In accord with experiment, the calculations predict that the ASIC SF is selective for Na^+ over both K^+ and Ca^{2+} and is more Na^+/Ca^{2+}-selective than Na^+/K^+-selective (more negative $\Delta G^{10}/\Delta G^{30}$ in Figures 4b,c than in Figure 4a). Indeed, the experimentally measured permeability ratios for the ASIC1a channel reveal that the Na^+-selective pore is less permeable to Ca^{2+} (Na^+:Ca^{2+} permeability ratio = 18.5) than to K^+ (Na^+:K^+ permeability ratio = 7.8)[8]. The model ENaC SF is also found to be much more discriminatory toward Ca^{2+} than K^+ (the $Na^+ \rightarrow Ca^{2+}$ ΔG^x numbers are an order of magnitude more negative than the $Na^+ \rightarrow K^+$ ΔG^x in Figure 5). This is in line with the experimental finding that ENaC exhibits a Na^+:K^+ permeability ratio of 100–500[3,11], but Ca^{2+} is *not* permeable[11]. The calculations also predict that a rigid ENaC SF (numbers in parentheses, Figure 5) is much more selective for Na^+ over K^+ and Ca^{2+} than its ASIC counterpart (which exhibits less negative ΔG^x values). This is in agreement with the greater Na^+:K^+ permeability ratio for the ENaC (100–500)[3,11] compared to that for the ASICs (3–30)[8,9], and the fact that ENaC is impermeable to Ca^{2+}, but the ASIC1A is slightly permeable to Ca^{2+}.

Selectivity in the large ASIC1a pore is not solely based on the hydrated ion size and its compatibility with the SF pore size[10]. Rather, it is a fine balance between electronic effects, which favor the cation that is a better electron acceptor (i.e., $Ca^{2+} > Na^+ > K^+$) and solvation effects, which favor the ion with smaller dehydration penalty binding (i.e., $K^+ > Na^+ > Ca^{2+}$). Electronic factors favor Na^+ over K^+ in the ASIC1a SF, because the shorter and more polar $Na–OH_2$ bonds compared to $K^+–OH_2$ bonds enable more hydrogen-bond contacts and stronger electrostatic interactions with the ligands lining the ASIC1a SF (Figure 4a). On the other hand, solvation effects favor binding of Na^+ over Ca^{2+} because Na^+ has a much smaller dehydration penalty than Ca^{2+} (Figure 4c). Changes in the metal hydration number inside the ASIC1a SF could be considered a second-order selectivity determinant. Consistent with the fact that hydrated Na^+ as well as the bulkier Cs^+ can be bound to the ASIC1a SF in the crystal structure, the pore rigidity does not play a major role in controlling metal ion competition, unlike the narrower ENaC SF pores (see below).

Compared to the ASIC1a SF, the ENaC SF has adopted a different selectivity strategy to achieve Na^+ selectivity[36]: Unlike the ASIC1a SF, the ENaC SF has a narrow and rigid pore that fits dehydrated metal ions, which bind directly to three SF ligands (Figure 5). Protein matrix effects that rigidify and constrict the SF pore so that the bulkier K^+ cannot fit optimally help to achieve high Na^+/K^+ selectivity. This is in line with experimental studies showing that the ENaC pore is rigid and narrow: In the series of monovalent ions, Na^+, K^+, Rb^+, Cs^+, NH_4^+, $(CH_3)NH_3^+$, $(CH_3)_2NH_2^+$, $(CH_3)_3NH^+$, and guanidine, the ENaC channel is permeable to only Na^+ and impermeable to the larger cations[33]. Backbone oxygen atoms interacting with the permeating ion in lieu of the weaker metal-ligating Ser hydroxyl group would further enhance Na^+/K^+ selectivity. This is consistent with mutagenesis data suggesting that a conserved Gly from the β subunit of the ENaC SF is important in restricting K^+ permeation[32]. On the other hand, the filter's trimeric structure and absence of strong metal-ligating groups such as Asp/Glu carboxylates favor Na^+ over Ca^{2+}. Thus, the pore's rigidity and undercoordination of the permeable ion by only three weak metal-ligating SF groups appear to be the key selectivity determinants of the ENaC SF (see Figure 5 and Ref. 24). Departing from these physical principles in the case of the ASIC1a SF; i.e., a hydrated metal ion with coordination number of six bound to a large and less rigid pore, diminishes the Na^+/K^+ and Na^+/Ca^{2+} selectivity and renders the ASIC channels less Na^+ selective than their ENaC counterparts (see above).

Methods

Selectivity Filter Models. Since crystallographic studies indicate a ASIC1a SF providing a ring of three carbonyl oxygen atoms with a pore radius that matches hydrated cations[12], we modeled hydrated cations bound in a SF containing three –$CONHCH_3$, representing peptide backbone groups (see Figures 1–4). On the other hand, experimental studies indicate that the ENaC transports completely dehydrated ions[37], but there is no consensus as to whether the backbone carbonyl or Ser hydroxyl oxygen atoms line a trimeric ENaC SF[30–32]. Hence, we modeled dehydrated metal cations bound in both **BBB** and **SSS** SFs lined with three –$CONHCH_3$ and three –OH groups, respectively (Figure 5). Models of the SFs were built using GaussView version 3.09 following the guidelines from our previous work[23]. The metal ligating groups were coordinated to the permeating bare/hydrated ion (Na^+, K^+ or Ca^{2+}) and attached to a carbon–hydrogen ring scaffold via flexible methylene spacers.

Justification of the Model SF Structures. The models of the ASIC1a and ENaC SFs were designed to maximize their resemblance with the channel's SF. They were constructed on the basis of the following considerations: (a) The ring mimics the oligomeric state and overall symmetry of the ion channel pore. (b) The ring scaffold prevents the metal ligands from drifting away or assuming unrealistic, pore-occluding positions during geometry optimization. If the metal ligands were detached from the ring scaffold, the fully optimized structure of the resulting metal-ligand complex would lose the pore-like shape, as one or more ligands would be positioned along the ion permeation pathway, thus occluding the pore[35]. Hence, the ring scaffold reflects the effects of the protein matrix in orienting the metal-ligating groups to interact with the permeating ions without obstructing the conduction pathway. (c) The metal-ligating groups and their connection to the ring are flexible enough to allow them to optimize their positions upon metal binding: the optimized metal–O distances in the model SF complexes were similar to those in metal complexes containing the free ligands without the ring scaffold[23]. (d) The shape and C–H orientations of the ring do not obstruct the pore lumen. Notably, the metal–O distances and pore sizes of the model SFs were found to be consistent with experimental estimates, as discussed above.

Gas-Phase Free Energy Calculations. Among several combinations of different ab initio/density functional theory methods (HF, MP2, S-VWN and B3-LYP) and basis sets (6-31+G(d,p), 6-31+G(2d,2p), 6-31+G(3d,p), 6-31+G(3d,2p), 6-311++G(d,p) and 6-311++G(3df,3pd)), the B3-LYP/6-31+G(3d,p) method has been shown to be the most efficient in yielding dipole moments of the metal ligands that are closest to the respective experimental values; it can also reproduce (within experimental error) the metal–oxygen bond distances in aqua and crown ether complexes, which resemble metal-occupied ion channel pores[23]. Hence, the B3-LYP/6-31+G(3d,p) method was used to optimize the geometry of each metal complex and to compute the electronic energies, E_{el}, using the Gaussian 09 program. Frequency calculations for each optimized structure were performed at the same level of theory. No imaginary frequency was found for the lowest energy configurations of the optimized structures. The B3-LYP/6-31+G(3d,p) frequencies were scaled by an empirical factor of 0.9613[38] and used to compute the thermal energies (E_{th}), including zero-point energy, and entropies (S). The differences ΔE_{el}, ΔE_{th}, ΔPV (work term) and ΔS between the products and reactants in eq 1 were used to calculate the gas-phase ΔG^1 free energy at T= 298.15 K according to:

$$\Delta G^1 = \Delta E_{el} + \Delta E_{th} + \Delta PV - T\Delta S \quad (3)$$

Solution Free Energy Calculations. The ΔG_{solv}^x (x = 10 or 30) values were estimated by solving Poisson's equation using finite difference methods[39,40] with the MEAD

(Macroscopic Electrostatics with Atomic Detail) program[41], as described in previous works[42]. Natural Bond Orbital atomic charges, which are known to be numerically quite stable with respect to basis set changes[43], were employed in the calculations. The effective solute radii were obtained by adjusting the CHARMM (version 22)[44] van der Waals radii to reproduce the experimental hydration free energies of Na^+, K^+ and Ca^{2+}, and model ligand molecules to within 1 kcal/mol[23,35,45]. The resulting values (in Å) are: $R_{Na} = 1.72$, $R_K = 1.90$, $R_{Ca} = 1.75$, $R_C = 1.95$, $R_N = 1.75$, $R_O(-CONHCH_3) = 1.72$, $R_O(H_2O) = 1.85$, $R_O(-CH_2OH) = 1.90$, $R_H = 1.50$, $R_O(Na/K–H_2O) = 1.85$, $R_O(Ca–H_2O) = 1.84$, $R_H(H_2O-Na) = 1.26$, $R_H(H_2O-K) = 1.20$, $R_H(H_2O-Ca) = 1.053$.

1. Kellenberger, S. & Schild, L. Epithelial sodium channel/degenerin family of ion channels: a variety of functions for a shared structure. *Physiol. Rev.* **82**, 735–767 (2002).
2. Grunder, S. & Chen, X. Structure, function, and pharmacology of acid-sensing ion channels (ASICs): focus on ASIC1a. *Int. J. Physiol. Pathophysiol. Pharmacol.* **2**, 73–94 (2010).
3. Kashlan, O. B. & Kleyman, T. R. ENaC structure and function in the wake of a resolved structure of a family member. *Am. J. Physiol. Renal Physiol.* **301**, F684–F696 (2011).
4. Krishtal, O. A. & Pidoplichko, V. I. A receptor for protons in the nerve cell membrane. *Neuroscience* **5**, 2325–2327 (1980).
5. Xiong, Z. G. *et al.* Neuroprotection in ischemia: blocking calcium-permeable acid-sensing ion channels. *Cell* **118**, 687–698 (2004).
6. Wemmie, J. A., Price, M. P. & Welsh, M. J. Acid-sensing ion channels: advances, questions and therapeutic opportunities. *Trends Neurosci.* **29**, 578–586 (2006).
7. Waldmann, R. Proton-gated cation channels - neuronal acid sensors in the central and peripheral nervous system. *Adv. Exp. Med. Biol.* **502**, 293–304 (2001).
8. Bassler, E.-L., Jennifer Ngo-Anh, T., Geisler, H.-S., Peter Ruppersberg, J. & Grunder, S. Molecular and functional characterization of acid-sensing ion channel (ASIC) 1b. *J. Biol. Chem.* **276**, 33782–33787 (2001).
9. Baconguis, I. & Gouaux, E. Structural plasticity and dynamic selectivity of acid-sensing ion channel-spider toxin complexes. *Nature* **489**, 400–406 (2012).
10. Yang, L. & Palmer, L. G. Ion conduction and selectivity in acid-sensing ion channel 1. *J. Gen. Physiol.* **144**, 245–255 (2014).
11. Palmer, L. G. Ion selectivity of the apical membrane Na channel in the toad urinary bladder. *J. Membr. Biol.* **67**, 91–98 (1982).
12. Baconguis, I., Bohlen, C. J., Goehring, A., Julius, D. & Gouaux, E. X-Ray structure of acid-sensing ion channel 1–snake toxin complex reveals open state of a Na^+-selective channel. *Cell* **156**, 717–729 (2014).
13. Nightingale Jr., E. R. Phenomenological Theory of Ion Solvation. Effective Radii of Hydrated Ions. *J. Phys. Chem.* **63**, 1381–1387 (1959).
14. Mahler, J. & Persson, I. A study of the hydration of the alkali metal ions in aqueous solution. *Inorg. Chem.* **51**, 425–438 (2012).
15. Marcus, Y. Ionic radii in aqueous solutions. *Chem. Rev.* **88**, 1475–1498 (1988).
16. Dudev, M., Wang, J., Dudev, T. & Lim, C. Factors Governing the Metal Coordination Number in Metal Complexes From Cambridge Structure Database Analyses. *J. Phys. Chem. B* **110**, 1889–1895 (2006).
17. Varma, S. & Rempe, S. B. Tuning ion coordination architectures to enable selective partitioning. *Biophys. J.* **93**, 1093–1099 (2007).
18. Varma, S., Sabo, D. & Rempe, S. B. K^+/Na^+ selectvity in K channels and valinomycin: Over-coordination versus cavity-size constraints. *J. Mol. Biol.* **376**, 13–22 (2008).
19. Dudev, T. & Lim, C. Metal selectivity in metalloproteins: Zn^{2+} vs. Mg^{2+}. *J. Phys. Chem. B* **105**, 4446–4452 (2001).
20. Babu, C. S., Dudev, T., Casareno, R., Cowan, J. A. & Lim, C. A Combined Experimental and Theoretical Study of Divalent Metal Ion Selectivity and Function in Proteins: Application to E-Coli Ribonuclease H1. *J. Am. Chem. Soc.* **125**, 9318–9328 (2003).
21. Dudev, T. & Lim, C. Bidentate vs. Monodentate Carboxylate Coordination Modes in Magnesium and Calcium Proteins: What are the Basic Principles? *J. Phys. Chem. B* **108**, 4546–4557 (2004).
22. Dudev, T., Chang, L.-Y. & Lim, C. Factors Governing the Substitution of La^{3+} for Ca^{2+} and Mg^{2+} in Metalloproteins: A DFT/CDM Study. *J. Am. Chem. Soc.* **127**, 4091–4103 (2005).
23. Dudev, T. & Lim, C. Determinants of K^+ vs. Na^+ selectivity in potassium channels. *J. Am. Chem. Soc.* **131**, 8092–8101 (2009).
24. Dudev, T. & Lim, C. Factors governing the Na^+ vs. K^+ selectivity in sodium ion channels. *J. Am. Chem. Soc.* **132**, 2321–2332 (2010).
25. Dudev, T. & Lim, C. Competition between Li^+ and Mg^{2+} in Metalloproteins. Implications for Lithium Therapy. *J. Am. Chem. Soc.* **133**, 9506–9515 (2011).
26. Dudev, T. & Lim, C. Importance of metal hydration on the selectivity of Mg^{2+} vs. Ca^{2+} in magnesium ion channels. *J. Am. Chem. Soc.* **135**, 17200–17208, doi:10.1021/ja4087769 (2013).
27. Dudev, T. & Lim, C. Evolution of eukaryotic ion channels: Principles underlying the conversion of Ca^{2+}-Selective to Na^+-selective channels. *J. Am. Chem. Soc.* **136**, 3553–3559, doi:10.1021/ja4087769 (2014).
28. Kuppuraj, G., Dudev, M. & Lim, C. Factors Governing Metal–Ligand Distances and Coordination Geometries of Metal Complexes. *J. Phys. Chem. B* **113**, 2952–2960 (2009).
29. Shannon, R. D. Revised effective ionic radii and systematic studies of interatomic distances in halides and chalcogenides. *Acta Crystallogr. A* **32**, 751–767 (1976).
30. Snyder, P. M., Olson, D. R. & Bucher, D. B. A pore segment in DEG/ENaC Na^+ channels. *J. Biol. Chem.* **274**, 28484–28490 (1999).
31. Kellenberger, S., Gautshi, I. & Schild, L. A single point mutation in the pore region of the epithelial Na^+ channel changes ion selectivity by modifying molecular sieving. *Proc. Natl. Acad. Sci. U.S.A.* **96**, 4170–4175 (1999).
32. Sheng, S., Perry, C. J., Kashlan, O. B. & Kleyman, T. R. Side chain orientation of residues lining the selectivity filter of epithelial Na^+ channels. *J. Biol. Chem.* **280**, 8513–8522 (2005).
33. Kellenberger, S., Auberson, M., Gautschi, I., Schneeberger, E. & Schild, L. Permeability properties of ENaC selectivity filter mutants. *J. Gen. Physiol.* **118**, 679–692 (2001).
34. Dudev, T. & Lim, C. Metal Binding and Selectivity in Metalloproteins: Insights from Computational Studies. *Annu. Rev. Biophys.* **37**, 97–116 (2008).
35. Dudev, T. & Lim, C. Competition among Ca^{2+}, Mg^{2+}, and Na^+ for ion channel selectivity filters: Determinants of metal ion selectivity. *J. Phys. Chem. B* **116**, 10703–10714 (2012).
36. Dudev, T. & Lim, C. Ion Selectivity Strategies of Sodium Channel Selectivity Filters. *Acc. Chem. Res.* **47**, 3580–3587 (2014).
37. Kellenberger, S. & Schild, L. Structure, function, and pharmacology of acid-sensing ion channels and the epithelial Na^+ channel. *Pharmocol. Rev.* **67**, 1–35 (2015).
38. Wong, M. W. Vibrational frequency prediction using density functional theory. *Chem. Phys. Lett.* **256**, 391–399 (1996).
39. Gilson, M. K. & Honig, B. H. Calculation of the electrostatic potential in solution: Method and error assessment. *J. Comp. Chem.* **9**, 327–335 (1988).
40. Lim, C., Bashford, D. & Karplus, M. Absolute pKa Calculations with continuum dielectric methods. *J. Phys. Chem.* **95**, 5610–5620 (1991).
41. Bashford, D. *Scientific Computing in Object-Oriented Parallel Environments.* (Springer, Berlin, 1997).
42. Dudev, T. & Lim, C. A DFT/CDM Study of Metal-Carboxylate Interactions in Metalloproteins: Factors Governing the Maximum Number of Metal-Bound Carboxylates. *J. Am. Chem. Soc.* **128**, 1553–1561 (2006).
43. Reed, A., Weinstock, R. & Weinhold, F. Natural population analysis. *J. Chem. Phys.* **83**, 735–746 (1985).
44. Brooks, B. R. *et al.* CHARMm: A program for macromolecular energy, minimization, and dynamics calculations. *J. Comput. Chem.* **4**, 187–217 (1983).
45. Dudev, T. & Lim, C. Why voltage-gated Ca^{2+} and bacterial Na^+ channels with the same EEEE motif in their selectivity filters confer opposite metal selectivity. *Phys. Chem. Chem. Phys.* **14**, 12451–12456, doi:10.1039/C2CP00036A (2012).

Acknowledgments

This work was supported by Academia Sinica, MOST, Taiwan (Grant NSC-98-2113-M-001-011). T.D. is supported by the Institute of Biomedical Sciences at Academia Sinica and EU Grant "Beyond Everest", FP7-REGPOT-2011-1.

Author contributions

T.D. performed the calculations. T.D. and C.L. designed the project and wrote the manuscript text. All authors reviewed the manuscript.

Additional information

Competing financial interests: The authors declare no competing financial interests.

How to cite this article: Dudev, T. & Lim, C. Ion Selectivity in the Selectivity Filters of Acid-Sensing Ion Channels. *Sci. Rep.* **5**, 7864; DOI:10.1038/srep07864 (2015).